ACS APPLIED MATERIALS & INTERFACES

Research Article

www.acsami.org

# Stress Generation and Tailoring of Electronic Properties of Expanded Graphite by Click Chemistry

Titash Mondal,[†] Anil K. Bhowmick,*[,†] and Ramanan Krishnamoorti*[,‡]

[†]Department of Chemistry, Indian Institute of Technology Patna, Patna, Bihar 800013, India

[‡]Department of Chemical and Biomolecular Engineering, University of Houston, Houston, Texas 77204, United States

Supporting Information

**ABSTRACT:** The generation of stress in expanded graphite (E-GPT) due to covalent attachment of bulky side groups connected via a hetero atom is reported. Specifically, E-GPT is modified at different levels of grafting using "click" chemistry to graft 1-ethynyl-4-fluoro benzene onto graphene sheets via a triazole ring. In the range of grafting densitites examined, Raman spectroscopy indicates that the stress generated in graphene is linearly dependent on the extent of grafting. The functionalized graphene platelets with 6% functionalization transform from semi-metal behavior of the pristine material to semi-conductor behavior and indicates the ability of functionalization to change optical and electronic properties of graphene platelets similar to the deposition of thin layers of top gate oxides onto graphene.


**KEYWORDS:** *graphene, click chemistry, stress, Raman spectroscopy, scanning tunneling microscopy*

## INTRODUCTION

The atomically thin dimensions along with the ability to ballistically transport electrons make graphene an important material especially for electronic applications.[1,2] However, the zero band gap structure of graphene often limits its usage for electronic applications.[3,4] Issues such as high off-state leakage current and non-saturating drive current are expected to be associated with graphene based devices such as transistors.[5,6] Thus, in order to make it a material of same caliber as silicon, engineering of the band gap of graphene becomes essential.[7−12] Some of the commonly used techniques to engineer the band-gap includes use of top gate oxides to induce stress on graphene[13] and applications of external bias onto bilayer graphene.[14] Other widely used methods for engineering of band gap of graphene are via integrating graphene surface with various dopant and metal atom.[15] However, the performance of graphene based devices and circuits are compromised.[16]

Covalent modification on the basal plane and the edges of graphene sheets and expanded graphite are also used as a convenient route for tuning the band gap of graphitic materials. Covalent functionalization techniques such as grafting of aryl group,[8] oxidation,[17] hydrogenation,[18−24] and fluorination of graphitic material[25−31] are often adopted. Structural inhomogeneity introduced in graphitic structure due to grafting of different functional group when modified by aryl group (problem of self-polymerization of aryl group)[32] or by oxidation method (various functional groups including carboxylic, epoxy, and hydroxyl groups are generated on the graphitic surface) affects the energy profile of graphitic material.[16] This makes such type of functionalized graphitic material unacceptable for use in electronic applications, for which structurally well-defined crystalline graphitic materials are required. Further, in most of the work reported in literature, CVD grown graphene or graphene nanoribbons are selected as a precursor material. However, reports on band gap engineering of graphitic material from expanded graphite are few.[15]

In this report, we adopted expanded graphite (E-GPT) as the precursor material. Further, we modulated the band gap of E-GPT in a simple approach by edge specific covalent modification with a triazole ring connected to a fluoro benzene unit. The edge specific covalent functionalization of E-GPT with different grafting densities was achieved using "click" chemistry.[33] The bulky functional group grafted onto the graphitic edges exerted stress onto the graphitic structure. While the edge selective modification of graphitic material using click chemistry has been reported,[34] there has been no report on the relationship between the stress generated and the levels of grafting achieved. Herein, we demonstrate a relationship by performing a systematic study using Raman spectroscopy. Biaxial compressive stress values of ∼1.60 GPa were observed for the highest level of grafting. Further, the effect of such kind of biaxial compressive stress on the band gap of graphene platelets was also evaluated using scanning tunneling spectroscopy (STS). A transition from semi-metallic behavior (pristine material) to semi-conductor nature (functionalized graphene platelets) was observed. This is due to the formation of carbon nitrogen single bond. The triazole ring so formed from the edges of graphene platelets introduced n-type

Received: January 22, 2014
Accepted: April 28, 2014
Published: April 28, 2014

   dx.doi.org/10.1021/am500471q | ACS Appl. Mater. Interfaces 2014, 6, 7244−7253

**Scheme 1. Proposed Scheme for the Modification of Expanded Graphite by Click Chemistry**

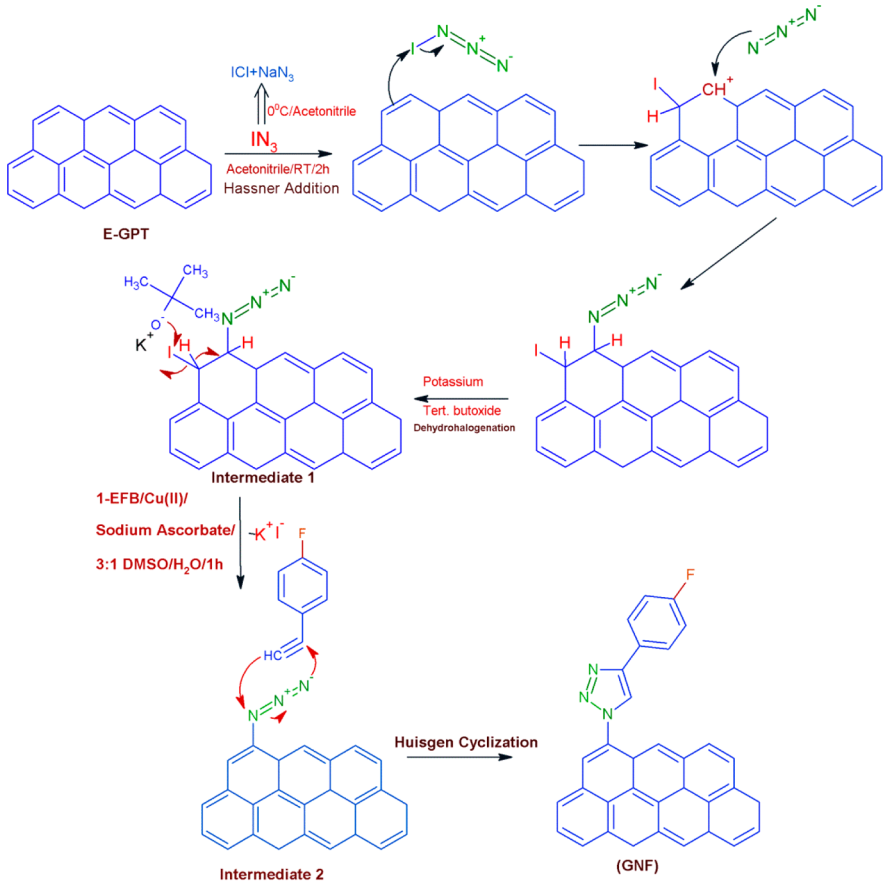


doping character. Reports on such type of doping phenomenon are documented in literature.[35,36] This work demonstrated the development of engineered band-gap materials prepared under mild reaction condition and minimal chemical usage and clearly distinguishes them from traditional preparation of semiconductor devices.

## EXPERIMENTAL SECTION

**Modification of Expanded Graphite by Click Chemistry.** A top down approach was adopted for synthesis of functionalized graphene platelets from E-GPT. The current synthesis method involved two steps. The first step involved generation of azide functionalized graphene nanoplatelets (-AG-) and the second step dealt with the modification of -AG- with 1-ethynyl-4-fluorobenzene (1-EFB). The iodine azide required in the first step of reaction (as shown in Scheme 1) was generated *in situ*. Three different sets of iodine azide was prepared by mixing 0.010, 0.020, and 0.030 g of sodium azide with iodine monochloride (0.006, 0.013, and 0.020 g) in 10 mL of acetonitrile at 0 °C. Further, these iodine azide solutions were introduced in three different sets of round bottom flask containing 0.25 g of E-GPT in 10 ml of acetonitrile. These reaction mixtures were warmed to room temperature, and they were kept for homogenization for 2 h in the presence of potassium tert-butoxide. The product so generated was filtered using 0.22 $\mu$m poly-tetra-fluoro ethylene (PTFE) filter membrane. To remove all of the unreacted starting materials and reaction by products, the isolated product was washed with acetonitrile followed by water and dried for further reaction. Three different level of azide grafted graphene platelets $(AG)_{0.5}$, $(AG)_1$, and $(AG)_2$ were obtained, with the subscript representing the level of functionalization.

In order to carry out the second step of reaction, azide modified graphene platelet surface, $(AG)_{0.5}$ was introduced to 20 $\mu$M 1-ethynyl-4-fluoro benzene in the presence of 0.4 mM of Cu(II)(tris-(benzyltriazolyl-methyl)amine)$SO_4$ and 16 mM sodium ascorbate. A 3:1 dimethyl sulfoxide/water mixture was used as the solvent for this reaction. The reaction was kept for 1 h at room temperature. The product, $(GNF)_{0.5}$ was isolated by doing filtration using 0.22 $\mu$m PTFE filter membrane. The isolated product was washed with water repeatedly to ensure proper removal of un-reacted starting materials and dried in a vacuum oven for further analysis. Similarly, $(AG)_1$ and $(AG)_2$ was introduced to 40 and 60 $\mu$M 1-ethynyl-4-fluoro benzene in the presence of 0.8 mM and 1 mM of Cu(II)(tris(benzyltriazolyl-methyl)amine)$SO_4$ and 32 mM and 40 mM sodium ascorbate in a 3:1 dimethyl sulfoxide/water mixture to generate $(GNF)_1$ and $(GNF)_2$. Further, the products obtained were isolated by doing filtration using 0.22 $\mu$m PTFE filter membrane. They were washed with water repeatedly to ensure proper removal of un-reacted starting materials and dried in a vacuum oven for further analysis.

**Characterization.** Fourier transform infrared (FTIR) spectroscopy was done using a Perkin Elmer 400 FTIR machine adopting a KBr pellet mode with a resolution of 2 $cm^{-1}$. X-ray photoelectron spectroscopy (XPS) measurements were made using a VG scientific ESCA Lab II Spectrometer with an electrostatic lens mode with pass energy of 160 eV with Mg K$\alpha$ radiation as an excitation source. The powder X-ray diffraction (XRD) patterns for the E-GPT and the modified graphene platelet were obtained using a Rigaku TT RAX 3 XRD machine with a Cu target (Cu K$\alpha$ radiation with $\lambda$ 0.154 nm) in the range of 2$\theta$ from 10−60°. The calculation of crystallite size and the micro strain introduced in the system after modification were assessed employing Rietveld technique using the Rigaku PDXL software after refinement of various structures including lattice parameters, peak width and shape, and preferred orientation. To quantify the grafting procedure, thermogravimetric analysis (TGA) was done in an inert atmosphere ($N_2$ gas) from room temperature to 800 °C with a ramp rate of 10 °C/min (SD Q600 TA Instruments). Atomic force


dx.doi.org/10.1021/am500471q | ACS Appl. Mater. Interfaces 2014, 6, 7244−7253

microscopy (AFM) was done in contact mode on freshly cleaved highly oriented pyrolytic graphite (HOPG) surface using silicon nitride tip for the pristine as well as the modified materials using Agilent AFM 5500. Height profiling across the E-GPT and modified graphene platelet was done using Agilent Pico image software. Characterization techniques such as FTIR, XPS, XRD, AFM, STM, and STS were carried out with optimized sample $(GNF)_1$.

**Raman Spectroscopic Measurement.** In order to analyze the defects formed due to grafting, both the pristine as well as the modified materials were characterized by Raman spectra using STR 750 series (Technos Instrument, India) Raman Spectrometer with 514.5 nm Ar-ion-laser source and grating of 600 lines/mm. Stress induced due to modification was also calculated utilizing Raman spectroscopy. In order to analyze the stress on the structure of modified graphene platelet, the samples were spin coated on glass coverslip (1 cm × 1 cm). The samples were placed on the sample stage and the laser focused on a specific area of the samples using 100× objective lens of attached microscope (Olympus BX-41) with a low laser power of around 1 mW. The Raman spectra were recorded at 10 different points. The results reported are an average of all the points.

**Scanning Tunneling Microscopic Analysis.** Scanning Tunneling Microscopic (STM) analysis (NanoRev 5.0, Quazar Technologies, India) was done with a bias voltage of −200 mV against a tunneling current of 300 pA using Pt/Ir tip. For STM analysis, briefly the modified samples were dispersed in acetone and further 2$\mu$L of that solution was drop casted on freshly cleaved HOPG surface. The sample was allowed to dry for 2 h so as to assure proper adherence of the modified material and complete evaporation of acetone. The current versus voltage ($I$–$V$) characteristics and the local density of states were also predicted using scanning tunneling spectroscopy (STS).

## RESULTS AND DISCUSSION

**Synthesis and Characterization of Modified Graphene Platelets.** When E-GPT was submerged in iodine azide solution, it was expected to undergo Hassner type of addition reaction.[37] The iodine moiety was anticipated to act as an electrophile and generate iodine functionalized graphitic intermediate. Further, the azide moiety reacted with the iodinated intermediate to form intermediate 1. However, in the presence of potassium tert-butoxide, it was predicted to undergo de-hydrohalogenation reaction. As a result, azide grafted graphene platelets were obtained (Scheme 1, intermediate 2). In order to support this proposition, FTIR spectroscopy was employed. E-GPT was devoid of any specific IR spectral features. However, the modified material, $(AG)_1$ had a signature peak due to the azide group at ∼2100 $cm^{-1}$ as shown Supporting Information Figure S1. Interestingly, iodine was reported to react at the least substituted carbon atom.[38] This made the edges of E-GPT as the dominant site for modification. Further, using a bulky base such as potassium tert-butoxide would increase the activation energy for the product predicted by Saytzeff's rule.[38] Thus, the sterically hindered base would scavenge proton from the less hindered site. This would give rise to the kinetically controlled product (Hoffman type).[38] From this proposed mechanism, we surmise that the azide moieties were grafted preferentially at the edges of E-GPT.

The pendant azide group grafted onto the edges of graphene platelets was not in a stable octet state. In order to achieve a stable octet state, the azide moiety would synchronously shift electrons to the dipolarophile for formation of 2$\sigma$ bonds. As a result when $(AG)_1$ was submerged in a solution containing 1-EFB, it readily reacted via 1,3 dipolar cycloaddition reaction, commonly known as Huisgen cyclization, as shown in Scheme 1.[39] Thus, the triazole ring formed, served as a pendant from the graphitic edges. In the range of variables and the experimental condition selected, restructuring of the graphitic framework and reaction with the azide nitrogen to produce nitrogen doped graphene (substitutional doping) was highly unexpected.

The isolated $(GNF)_1$ was further characterized by FTIR spectroscopy. As expected, the peak at ∼2100 $cm^{-1}$ disappeared as shown in Supporting Information Figure S1. However, new peaks were observed at 1261 $cm^{-1}$ and 1573 $cm^{-1}$ due to the formation of carbon−nitrogen bond and carbon−carbon double bond of the ring. An additional peak was observed at 1016 $cm^{-1}$ for $(GNF)_1$ and is attributed to the carbon−fluorine bond present in the modifier as shown in Figure 1. The

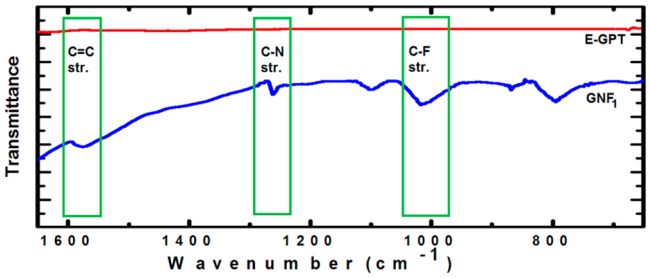


**Figure 1.** Selective region infrared spectra of E-GPT and $(GNF)_1$ performed in transmission mode using KBr pellet technique using 64 scans and a resolution of 2 $cm^{-1}$.

degree of functionalization was also estimated by techniques reported earlier.[40,41] Grafting densities ranging of 4.2%, 5.4%, and 5.8 % were obtained for $(GNF)_{0.5}$, $(GNF)_1$, and $(GNF)_2$ respectively (Supporting Information Figure S2).

In order to further quantify the functionalization, XPS was employed for both E-GPT and $(GNF)_1$ as shown in Figure 2. E-GPT was marked by its signature peak at 284.5 eV due to core C 1s electron. The presence of two deconvoluted peaks under C 1s peak for E-GPT was attributed due to the presence of graphitic carbon (284.5 eV) and the carbon atom bonded to hydroxyl functionality (285.6 eV), present in the starting material (Figure 2a). The single Gaussian peak at 532.5 eV was due to the presence of O 1s electrons from the hydroxyl functionality present in the starting material (Figure 2b). Thus, to quantify the oxygen content, calculation based on the area corresponding to the oxygen was done. The O/C ratio for G was found to be 2.6/97.4, where sensitivity factors of 0.66 for O 1s and 0.25 for C 1s were employed. XPS analysis of $(GNF)_1$ further confirmed the grafting process. Apart from the presence of graphitic carbon atom (284.5 eV), multiple deconvoluted peaks for C 1s were observed at 285.2 and 285.9 eV. These peaks were ascribed to covalent attachment of carbon to electronegative elements such as nitrogen and fluorine, respectively.[42] Attachment of electronegative species to carbon tends to decrease electron density of C 1s, which resulted in an increase in binding energy of carbon.[43] Further, high resolution XPS was also done for nitrogen and fluorine. The origin of three deconvoluted peaks for nitrogen at 398.7, 399.8, and 401.4 eV was due to the different chemical environment of nitrogen in triazole ring formed in $(GNF)_1$ as shown in Figure 2e. The percentage grafting for $(GNF)_1$ was assessed with the help of XPS analysis and found to be 5.1%. This was consistent with value obtained from FTIR spectroscopy.

Thermogravimetric analysis was done and was compared with that of E-GPT as shown in Figure 3. E-GPT lacks any

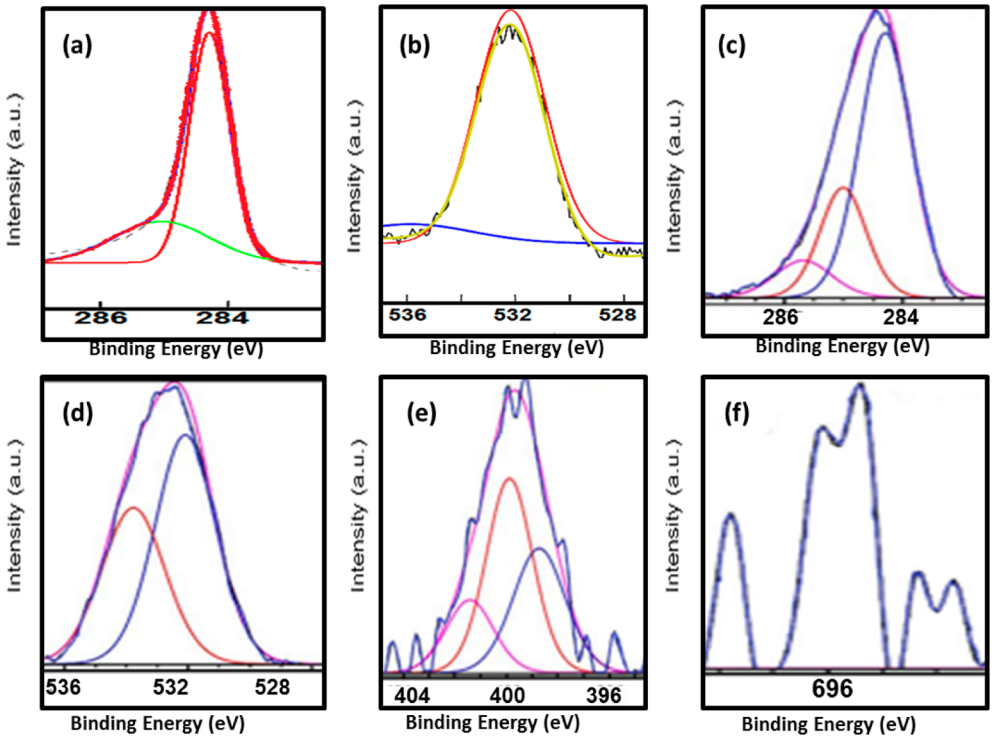


**Figure 2.** High resolution XPS spectra of (a) E-GPT C 1s, (b) E-GPT O 1s, (c) $(GNF)_1$-C 1s, (d) $(GNF)_1$-O 1s, (e) $(GNF)_1$-N 1s, and (f) $(GNF)_1$-F 1s. Mg K$\alpha$ radiation (Pass energy of 160 eV) was used as an excitation source for the experiment.

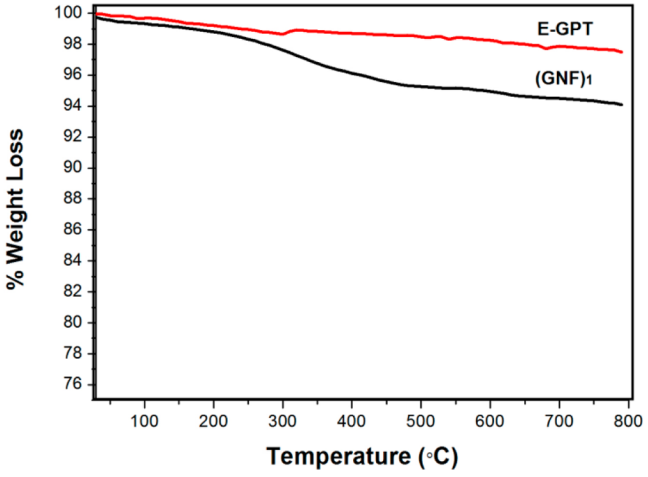


**Figure 3.** Thermogravimetric analysis of E-GPT and $(GNF)_1$ performed under nitrogen atmosphere using a ramp rate of 10 °C/min from room temperature to 800 °C.

noticeable weight loss during heating from room temperature to 800 °C (in $N_2$ condition) due to the absence of covalently attached functional groups. However, $(GNF)_1$ was associated with a total 6% weight loss under similar conditions. The weight loss observed in thermal analysis was consistent with grafting density inferred from the XPS analysis. The first step of degradation was noted in the TGA trace at 320 °C. This degradation was anticipated due to the scission of the carbon nitrogen single bond present between graphitic carbon and the triazole ring.

Further, AFM was employed in order to understand the structural changes that are taking place after functionalization. Using the contact mode of analysis, the lateral dimension for the pristine material was found to be around a few hundred nanometers, as shown in Figure 4a. Similarly, the $(GNF)_1$ was analyzed under identical conditions. Interestingly, the modified

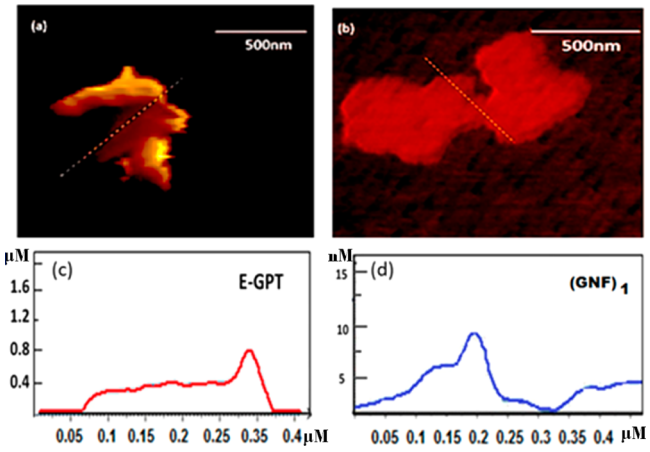


**Figure 4.** AFM topography of (a) E-GPT , (b) $(GNF)_1$ done using contact mode on freshly cleaved HOPG surface using silicon nitride tip, height profile across (c) E-GPT (scale in *X* and *Y* axes are in $\mu$M) and (d) $(GNF)_1$ (scale in *X* and *Y* axes are in $\mu$M and nM, respectively). The step height profiling was done using Agilent Pico image software.

material was found to be of similar lateral dimension (Figure 4b). This implies that the route selected for functionalization was mild enough in keeping the structural integrity of graphene intact. This also indicates about the consistency in the crystallite size of the modified graphene platelets with respect to the pristine graphite. There are reports in literature which claims that harsh functionalization methods disrupt the charge carrier ability of graphitic structure, which is highly undesirable in electronic applications.[44] Further, in our synthesis approach,


dx.doi.org/10.1021/am500471q | ACS Appl. Mater. Interfaces 2014, 6, 7244−7253

we have selected top down approach for synthesis of functionalized graphene platelets from expanded graphite. Thus, it is expected that functionalized product is expected to be de-laminated compared to pristine material. In order to quantify the extent of de-lamination phenomenon, height profiling was done across the E-GPT and $(GNF)_1$ by the procedure described elsewhere.[45] E-GPT was found to be around 400 nm thick (Figure 4c) whereas $(GNF)_1$ was observed to be ~10 nm thick (Figure 4d). The bulky functional group grafted onto graphene sheet is expected to act as a spacer. As a result, they will tend to repel each other and thereby preventing further stacking of graphene layers.

In order to observe the atomic structure present in the modified materials and to draw an analogy with the atomic pattern of pristine material, STM was employed using a procedure described elsewhere.[46] The $X-Y$ piezo of the STM was calibrated against the atomically resolved HOPG. Down to the atomic level, reproducible hexagonal patterns were observed for E-GPT (Figure 5a). For the pristine material,

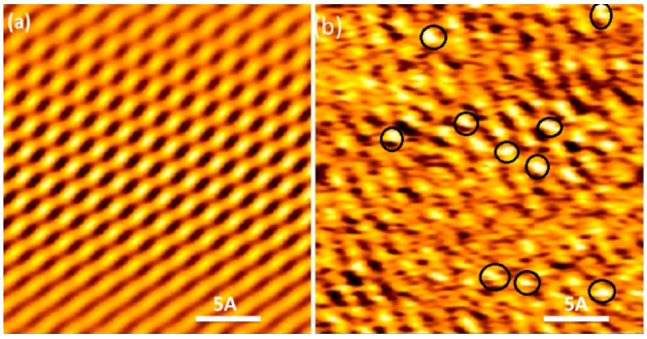


**Figure 5.** Atomic level image of (a) E-GPT. (Scan done at 25 × 25 Å area.) (b) $(GNF)_1$ (scan done at 25 × 25 Å area) done with a bias voltage of −200 mV against a tunneling current of 300 pA using Pt/Ir tip.

typical Moiré patterns were observed in the 2D FFT of the original image as reported in literature.[47] The bright and the dark spot for the pristine material appeared due to the high and low tunneling current across the surface. This was due to the typical three-dimensional spatial arrangement of the carbon atoms in E-GPT. This leads to a variable surface conductivity for graphite. The waviness around the edges of pristine material resulted in a distorted Moiré pattern as shown in Figure 5a. However, the surface feature for $(GNF)_1$ was found to be coarser compared to the pristine material. The 2D FFT image showed uneven Moiré pattern with interference over the entire image, as shown in Figure 5b. The low resolution of the STM image of $(GNF)_1$ was attributed to the decrease in the conductivity of the sample due to functionalization. Further, based on our hypothesis, the chemical functionalization was expected to take place at the edges of graphitic sheet. Any such modification at the edges of graphitic sheets, induces a stress at the graphtic edges.[48] This resulted in formation of ripples across the basal plane of graphene sheet.[48] As a result few bright spots were observed on the basal plane of $(GNF)_1$. Such observations made during STM analysis due to the presence of ripples across the basal plane of graphene sheet have been reported in the literature.[49,50]

Powder XRD was adopted in order to characterize the changes taking place in the lattice parameters for $(GNF)_1$ with respect to E-GPT. As shown in Figure 6a, an intense crystalline

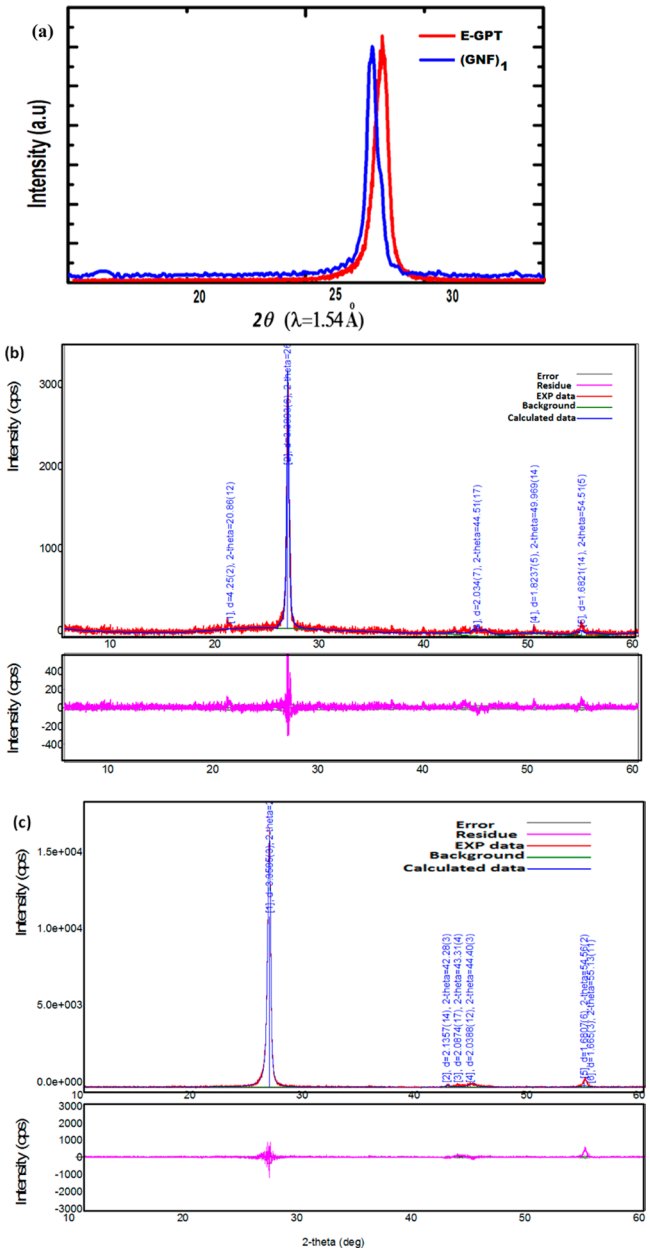


**Figure 6.** (a) Selective area wide angle powder XRD pattern for E-GPT and $(GNF)_1$ using a Cu K$\alpha$ radiation with $\lambda$ = 0.154 nm. (b, c) Rietveld refinement of XRD data for (b) $(GNF)_1$ and (c) E-GPT done using Rigaku PDXL software. The pristine and modified material was indexed against graphite 2H of space group *P*63/*mmc* from ICDD database. A pseudo-Voit function was used for approximation of the experimental XRD pattern.

peak was observed at 26.5° for E-GPT due to the graphitic [002] plane. However, the intense peak got shifted to 26.3° for $(GNF)_1$ owing to the functionalization taking place.

Further, Rietveld refinement was done using Rigaku PDXL software. The pristine and the modified material were indexed on the basis of graphite 2H with space group of P63/mmc from ICDD database as shown in Figure 6c.

A pseudo-Voit function was used for approximation of the experimental XRD pattern. Upon refinement, the *a*, *b*, and *c* lattice parameters for E-GPT were obtained as 0.247, 0.247, and 0.675 nm, respectively. However, the parameters for $(GNF)_1$ were changed to 0.240 nm (*a*), 0.240 nm (*b*), and


dx.doi.org/10.1021/am500471q | ACS Appl. Mater. Interfaces 2014, 6, 7244−7253

0.667 nm ($c$) due to the functionalization taking place. All the results are associated with 0.05% of error. Various statistical parameters involved in the Rietveld refinement are listed in Table 1.

**Table 1. Parameters from Rietveld Refinement**

| param. | E-GPT | $(GNF)_1$ |
|---|---|---|
| profile factor ($R_p$) | 15.49% | 20.94% |
| reliability factor ($\chi^2$) | 1.66 | 1.41 |
| goodness of fit ($S$) | 1.28 | 1.18 |

Apart from the change in peak position and lattice parameters, the other notable difference that was observed was the change in the full width at half maxima ($\Gamma$) for graphitic [002] peak. Under similar experimental conditions, (Cu-Anode; $\lambda$ = 0.154 nm), the $\Gamma$ value increased from 0.239° (E-GPT) to 0.256° for $(GNF)_1$. Based on the equation due to Stokes and Wilson (eq 1),[51] there are two controlling factors for peak broadening: (i) crystallite size ($D$) and (ii) micro-strain ($\varepsilon$).

$$\Gamma \cos\theta = \frac{k\lambda}{D} + \varepsilon \sin\theta \quad (1)$$

where $k$ is the shape factor taken as 0.9 and $\lambda$ is the wave length of incident X-ray beam used. However, in the present case, the consistency of the $D$ value (before and after modification, as observed from various microscopic techniques, *viz*, AFM) makes $\varepsilon$ as the governing factor for peak broadening. Thus, on the basis of the above eq 1 (using Rigaku PDXL software), the micro-strain values were calculated. The absolute internal micro-strain calculated using eq 1 in E-GPT was 0.0026 and increased to 0.0053 for $(GNF)_1$.

The origin of this micro-strain is attributed to the chemical functionalization. The modifier used for the functionalization of E-GPT comprises of a triazole ring connected to a substituted phenyl unit. This means that the lattice parameter for the modifying unit is different from that of E-GPT. As a result of such type of lattice mismatch, the functional group is expected to exert biaxial compressive stress onto graphene sheet. Further, based on the observation made from STM studies, there is presence of ripples on the basal plane of $(GNF)_1$. These ripples on the basal plane of graphene sheet are reported as the local site for development of strain.[52] Thus, even though we are modifying E-GPT at the edges, we are observing micro strain on the basal plane for $(GNF)_1$.

An estimation of the stress induced at the edges of $(GNF)_1$ can be obtained by noting the changes in the frequencies of the Raman $E_{2g}$ phonons of modified graphene platelets with respect to E-GPT. Raman spectroscopy is widely used for characterizing graphitic materials. The simplicity involved in spectral interpretation makes Raman spectroscopy a popular tool.[53] E-GPT exhibited finger print bands such as the G-band and D-band when subjected to 514.5 nm Ar ion source (as shown in Figure 7). In particular, the G-band, which is a marker for $sp^2$ hybridized carbon system, is primarily attributed to the $E_{2g}$ phonon mode located at the centre of Brillouin zone,[53,54] whereas the molecular basis of the D-band was ascribed to the defects induced in symmetrical hexagonal network of graphite. Here in the present case, the D and G bands were found to be at 1352 $cm^{-1}$ and 1563 $cm^{-1}$ for E-GPT. The $A_D/A_G$ ratio for E-GPT was found to be 0.22, where $A_D$ and $A_G$ are the area under the D and G bands of Raman spectra. The full width at

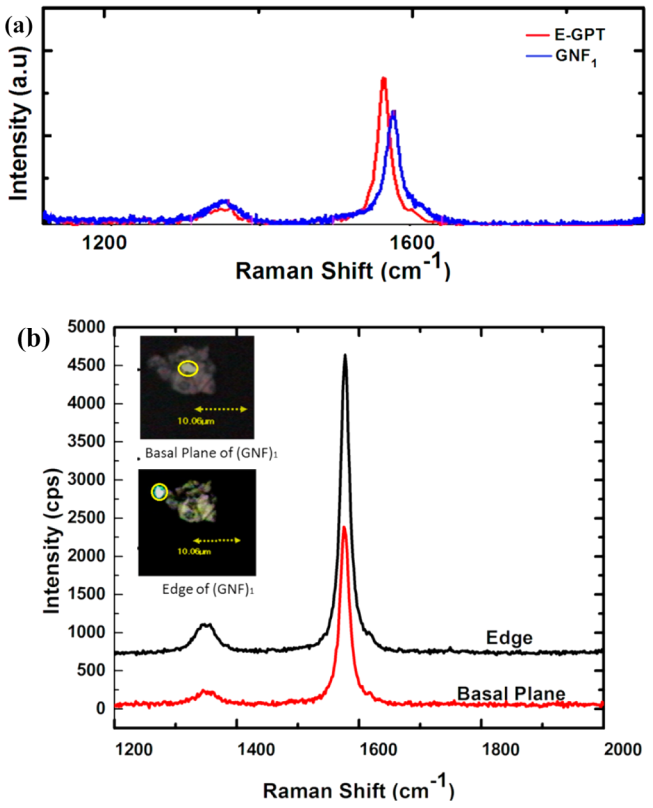


**Figure 7.** (a) Normalized Raman spectra of E-GPT and $(GNF)_1$ using 514.5 nm Ar ion laser source was recorded with a grating of 600 mm/lines. The G-band for E-GPT was recorded at 1563 $cm^{-1}$. The G-band was upshifted by 12 $cm^{-1}$ and was noted at 1575 $cm^{-1}$ for $(GNF)_1$. (b) $I_D/I_G$ ratio for $(GNF)_1$ was recorded at the basal plane (red line) as well as edges (black line) using 514.5 nm Ar ion laser source. 600 mm/lines grating was used for this experiment (Inset showing the Raman imaging of $(GNF)_1$ area from which the spectra has been recorded).

half maxima ($\Gamma$) for the G band was observed as 19.50 $cm^{-1}$. Under similar experimental conditions, the Raman spectra for $(GNF)_1$ was recorded. The D and the G band for $(GNF)_1$ were observed at 1353 $cm^{-1}$ and 1575 $cm^{-1}$, respectively. The $A_D/A_G$ ratio was found to be 0.37, which proved surface modification, as shown in Figure 7. The $\Gamma$ value observed for $(GNF)_1$ was 20.57 $cm^{-1}$. Two notable differences were observed when the Raman spectra for E-GPT and $(GNF)_1$ were compared: (i) G-band for $(GNF)_1$ was stiffer (up-shifted by 12 $cm^{-1}$) and broader compared to that for E-GPT, (ii) decrease in the relative intensity of G-band was observed compared to E-GPT (as shown in Figure 7a).

De-lamination of graphitic layers are reported to cause stiffening and broadening of the G-band.[55] Similarly, in the present case, the de-lamination of graphitic layers in case of $(GNF)_1$ compared to E-GPT (as observed from AFM step height measurment) resulted in peak stiffening and broadening of G-band. Further, it was also reported that presence of significant proportion of unmodified areas in the basal plane of graphene sheet often causes blue shift of the G-band.[55] This supports our observation made from TGA, wherein we have reported that 94% of the graphitic structure was unmodified. These observations can be justified based on the effect of covalent modification on the frequencies of in-plane transverse optic phonon (iTO) and longitudinal optical phonon (LO). The direct consequence of such modification is splitting of the


dx.doi.org/10.1021/am500471q | ACS Appl. Mater. Interfaces 2014, 6, 7244−7253

iTO and LO phonon frequencies. As a result, the G band is expected to be shifted and broadened.[56]

Further, from Raman spectroscopy, the contribution from basal plane as well as from the edges of graphitic sheet can be inferred. The ratio of $I_D/I_G$ acts as a marker for determining the extent of chemical modification taking place. As shown in Figure 7b, the Raman spectra was recorded at the basal plane and the edges of $(GNF)_1$.

The $I_D/I_G$ for the basal plane region was found to be 0.09, where the $I_D/I_G$ ratio for the edge region was found to be 0.3. Based on our hypothesis, chemical functionalization is expected to take place selectively around the edges. This will result in conversion of $sp^2$ hybridized carbon atom to $sp^3$ hybridized one at the edges. As a result, the $I_D/I_G$ ratio around the edges should be higher than that of the basal plane. This observation proves that the there is a preferential grafting of functional group is taking place at the edges of graphitic sheet compared to the basal plane. All the experiments were evaluated by taking the average of triplicate of experiments performed.

Moreover, grafting of functional group onto graphitic surfaces is expected to cause volume change in the system. Such volume changes can be related thermodynamically to Grüneisen parameter $(\gamma)$[56] as shown in eq 2.

$$\gamma = v\left(\frac{\partial P}{\partial E}\right)_P \tag{2}$$

where $v$ is the volume, $p$ is the pressure, and $E$ is the total energy of the system.

Further, this Grüneisen parameter can also be linked with frequencies of the phonons involved in the lattice by

$$\gamma = -\left(\frac{v}{\omega_0}\right)\left(\frac{\partial \omega_0}{\partial v}\right) \tag{3}$$

where $\omega_0$ is frequency of phonon of unstrained graphene crystal. For the present case, the Grüneisen parameter was calculated as[57]

$$\gamma = \left(\frac{\omega_\theta - \omega_0}{2\varepsilon\omega_0}\right) \tag{4}$$

where $\omega_\theta$ and $\omega_0$ are the Raman frequencies under strained and unstrained conditions for pristine and modified graphene platelets. The Grüneisen parameter for the optimized sample, $(GNF)_1$ was found to be 1.48 with respect to the shift in the G-band. Considering the errors associated with the Raman spectroscopic measurement, the $\gamma$ value was found to be consistent with values reported in literature.[58] Thus, with an increase in the grafting density, it is expected to have higher value of Grüneisen parameter. Based on the reports availabe in literature, the biaxial compressive stress can be calculated using eq 5[59] (Detailed calculation is provided in the Supporting Information, equation S1−S4):

$$(\omega_\theta - \omega_0) = \frac{2A(S_{11} + S_{12})}{2\omega_0}\sigma = \beta\sigma \tag{5}$$

where $\beta$ is the stress coefficient. Based on the values of parameter obtained from literature,[59] we assign $A = -1.44 \times 10^7$ cm$^{-2}$ and graphitic elastic constants $S_{11}$ and $S_{12}$ are $0.98 \times 10^{-12}$ Pa$^{-1}$ and $-0.16 \times 10^{-12}$ Pa$^{-1}$, respectively. Thus, using the above model, the shift in the position of the G band can be correlated with developed biaxial compressive stress after modification. From, application of eq 5, the compressive stress value obtained were 1.60 GPa (± 5 % error) for $(GNF)_2$; 1.58 GPa (± 5 % error) for $(GNF)_1$ and 1.06 GPa (± 5 % error) for $(GNF)_{0.5}$, respectively. Thus, by grafting a bulky functional group, a stress comparable to the one reported in a noncovalent route (deposition of top gate oxide) in literature can be generated onto graphene sheet for tuning its electronic properties.[13] In the noncovalent route reported, deposition of graphene sheet on a polymeric scaffold is performed and this scaffold is subjected to further mechanical strain. Generally, polymeric scaffolds are made out of poly-dimethylsiloxane (PDMS). However, the poor adhesion force acting between the un-functionalized graphene sheet and the polymeric scaffold due to the inherent elasticity of the polymer chains results in slippage in between them. As a result, an inefficient transfer of strain onto graphene is observed. Moreover, this technique involves curing of the liquid PDMS in the presence of graphene. As a result, there will be a volume contraction happening due to the curing process of the polymer. This will further induce strain onto the graphene sheet.[60] Additionally, the presence of isolated topological defects on the graphene structure imparts strain. Thus, even though in the non-covalent route the cumulative strain on graphene can be quantified by noting the changes in phonon frequencies, it is difficult to ascertain the percentage of strain contributed by each of the above mentioned factors. However, in the present chemical functionalization route, engineered stress can be generated as a function of the extent of modification. Here, the stress is transferred to the graphene sheet is a function of the modifying group. Hence, the problems which are commonly associated with the non-covalent route can be circumvented by this technique. Thus, based on the calculation of percent grafting from FTIR and the observation made in Raman spectroscopy, we can summarize them as shown in Figure 8. The stress generated in graphene platelets was linearly dependent on the extent of grafting in the range of grafting densitites examined.

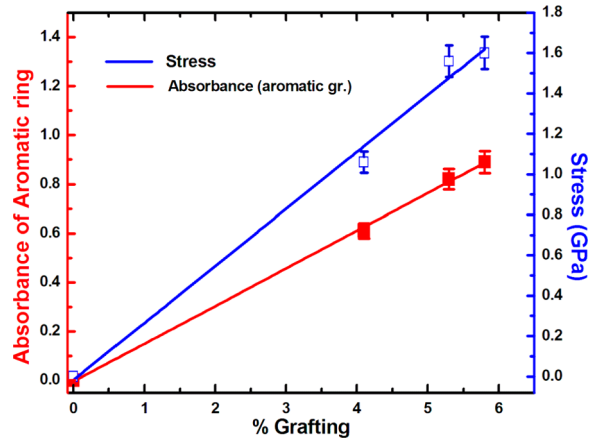


**Figure 8.** Correlation between stress generated, absorbance due to aromatic ring of grafted group and the extent of grafting.

The impact of the stress generated due to chemical modification of graphite on the local density of state was estimated and compared with that of pristine material using STS. The $I-V$ characteristics as well as the $d[\ln I]/d[\ln V]$ plot for E-GPT suggested about its semi metallic nature (Band gap of 0.02 eV), as shown Figure 9 and Supporting Information Figure S3. The reason for such an electronic behavior is attributed to its structure. Graphene with its protruding out of

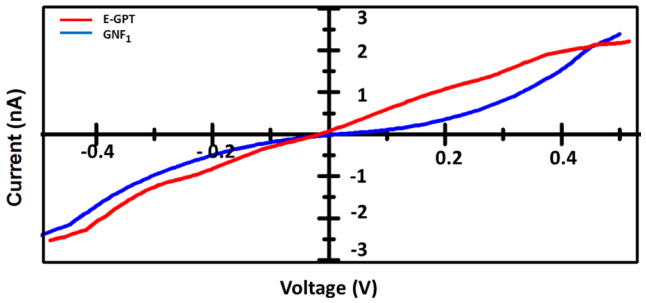


**Figure 9.** $I-V$ curve for E-GPT and $(GNF)_1$ as obtained from the STS measurement.

plane $2p_z$ orbital tends to interact with the adjacent $2p_z$ orbital of carbon atoms in adjacent graphene sheet. As a result, delocalized bonding ($\pi$) and anti-bonding ($\pi^*$) energy levels are generated. Further, considering the hexagonal Brillouin zone of graphene, these two energy states are found to be degenerate at the Dirac point. Since the environment of all the carbon atom are identical, these energy levels are linearly dispersed and they practically touch each other at the Dirac point. This causes graphene to have almost zero band gap structure and behave as a semi-metal. On the other hand, the modified material behaved more like a semi-conductor (Band gap of 0.2 eV), as shown in Supporting Information Figure S3. Any covalent modification of graphitic material is expected to cause potential redistribution of the surface charges. As a result, it is anticipated that the local structure of graphitic structure is significantly perturbed. This brings about changes at the Dirac point and causes a separation between the $\pi$ and $\pi^*$ energy levels. Additionally, in the present case, the modifier is linked to graphene platelets via carbon−nitrogen single bond. Differences in the electronegativity values for carbon and nitrogen is expected to generate dipole moment. This induced dipole moment will further facilitate destruction of the symmetry present in graphitic structure. As a result the band gap is expected to open up. Based on the above mentioned factors, the semi-conducting behavior of graphene platelets is not unexpected.

## SUMMARY

We have demonstrated that successful modification of E-GPT utilizing "click" chemistry was achieved and the extent of functionalization as determined by different techniques were in reasonable agreement. Generation of stress was also achieved by varying the degree of functionalization. Raman spectroscopy was employed to estimate the amount of stress generated due to modification. An atomic insight about the structure of the pristine and modified material was observed using STM. STS provided a detail nature of the electronic property of the pristine and the modified materials. The functional group attached to the E-GPT through the click chemistry acted as a n-type dopant. The electronegativity differences resulted in generation of dipoles. This causes a break in the local symmetry of graphitic network, thereby opening the band gap for the modified material. Due to this reason, a notable transition from semi-metallic to semi-conducting nature of the modified material was observed. Further, this strategy can be extended for grafting of bulky functional groups such as porphyrins, phthalocyanine for generation of tunable stress onto graphene.

## ASSOCIATED CONTENT

### Supporting Information

Selective area FTIR spectra, estimation of percentage grafting using FTIR spectroscopy, STS plot of $d[\ln I]/d[\ln V]$ versus voltage for pristine and modified material, and calculation of biaxial compressive stress using Raman spectroscopy is provided in the supporting information section. This material is available free of charge via the Internet at http://pubs.acs.org/

## AUTHOR INFORMATION

### Corresponding Authors

*Email: anilkb@rtc.iitkgp.ernet.in.
*Email: ramanan@uh.edu.

### Author Contributions

T.M. and A.K.B. designed the experiments. T.M. performed the experiments and analyzed the data. T.M., R.K., and A.K.B. contributed to the understanding of the results and the writing of the manuscript.

### Notes

The authors declare no competing financial interest.

## ACKNOWLEDGMENTS

This project was funded by Indian Institute of Technology Patna, India. T.M. thanks the Director, IIT Patna, for providing facilities to carry out the research work. R.K. acknowledges the partial support of the Gulf of Mexico Research Initiative (Consortium for Ocean Leadership Grant SA 12-05/GoMRI-002). The authors acknowledge Indo-US Science and Technology Forum (IUSSTF) for their support. T.M. and R.K. dedicate this paper to Prof. Anil Bhowmick on the occasion of his 60th birthday.

## REFERENCES

(1) Geim, A.K.; Novoselov, K.S. Rise of Graphene. *Nat. Mater.* **2007**, *6*, 183−191.
(2) Schweirz, F. Graphene Transistors. *Nat. Nanotechnol.* **2010**, *5*, 487−496.
(3) McCann, E. Asymmetry Gap in the Electronic Band Structure of Bilayer Graphene. *Phys. Rev. B* **2006**, *74*, 161403.
(4) Meric, I.; Han, M. Y.; Young, A. F.; Ozyilmaz, B.; Kim, P.; Shepard, K. L. Current Saturation in Zero Band Gap Top-Gated Graphene Field Effect Transistors. *Nat. Nanotechnol.* **2008**, *3*, 654−659.
(5) Banerjee, S. K.; Register, L. P.; Tutuc, E.; Kim, S.; Reddy, D.; MacDonald, A. H. Graphene for CMOS and Beyond CMOS Applications. *Proc. IEEE* **2010**, *98*, 2032−2046.
(6) Xia, F. N.; Farmer, D. B.; Lin, Y. M.; Avouris, P. Graphene Field-Effect Transistors with High On/Off Current Ratio and Large Transport Band Gap at Room Temperature. *Nano Lett.* **2010**, *10*, 715−718.
(7) Han, M. Y.; Ozyilmaz, B.; Zhang, Y.; Kim, P. Energy Band-Gap Engineering of Graphene Nanoribbons. *Phys. Rev. Lett.* **2007**, *98*, 206805.
(8) Zhou, S. Y.; Gweon, G.-H.; Fedorov, A. V.; First, P. N.; deHeer, W. A.; Lee, D.-H.; Guinea, A. H.; Castro Neto, A. H.; Lanzara, A. Substrate Induced Band Gap Opening of Epitaxial Graphene. *Nat. Mater.* **2007**, *6*, 770−775.
(9) Bekyarova, E.; Sarkar, S.; Wang, F.; Itkis, M. E.; Kalinina, I.; Tian, X.; Haddon, R. C. Effect of Covalent Chemistry on the Electronic Structure and Properties of Carbon Nanotubes and Graphene. *Acc. Chem. Res.* **2013**, *46*, 65−76.
(10) Shih, C.-J.; Wang, Q. H.; Jin, Z.; Paulus, G. L. C.; Blankschtein, D.; Herrero, P. J.; Strano, M. Disorder Imposed Limits of Mono- and

Bilayer Graphene Electronic Modification Using Covalent Chemistry. *Nano Lett.* **2013**, *13*, 809−817.
(11) Jung, S.-M.; Lee, E. K.; Choi, M.; Shin, D.; Jeon, I.-Y.; Seo, J.-M.; Jeong, H. Y.; Park, N.; Oh, J. H.; Baek, J. H. Direct Solvothermal Synthesis of B/N Doped Graphene. *Angew. Chem. Int. Ed.* **2014**, *9*, 2398−2401.
(12) Abbas, A. N.; Liu, G.; Liu, B.; Zhang, L.; Ohlberg, D.; Wu, W.; Zhou, C. Patterning, Characterization and Chemical Sensing Application of Graphene Nanoribbon Arrays down to 5 nm Using Helium Ion Beam Lithography. *ACS Nano* **2014**, *8*, 1538−1546.
(13) Ni, Z. H.; Wang, H. M.; Ma, Y.; Kasimand, J.; Shen, Z. X. Tunable Stress and Controlled Thickness Modification in Graphene by Annealing. *ACS Nano* **2008**, No. 2, 1033−1039.
(14) Castro, E. V.; Novoselov, K. S.; Morozov, S.V.; Peres, N. M. R.; Lopes dos Santos, J. M. B.; Nilsson, J.; Guinea, F.; Geim, A. K.; Castro Neto, A. T. T. Biased Bilayer Graphene: Semiconductor with a Gap Tunable by the Electric Field Effect. *Phys. Rev. Lett.* **2007**, *99*, 216802.
(15) Zhu, W.; Neumayer, D.; Perebeinos, V.; Avouris, P. Silicon Nitride Gate Dielectrics and Band Gap Engineering in Graphene Layers. *Nano Lett.* **2010**, *10*, 3572−3576.
(16) Johns, J. E.; Hersam, M. C. Atomic Covalent Functionalization of Graphene. *Acc. Chem. Res.* **2013**, *46*, 77−86.
(17) Hummers, W. S.; Offeman, R. E. Preparation of Graphitic Oxide. *J. Am. Chem. Soc.* **1958**, *80*, 1339−1339.
(18) Elias, D. C.; Nair, R. R.; Mohiuddin, T. M. G.; Morozov, S. V.; Blake, P.; Halsall, M. P.; Ferrari, A. C.; Boukhvalov, D. W.; Katsnelson, M. I.; Geim, A. K.; Novoselov, K. S. Control of Graphene's Properties by Reversible Hydrogenation: Evidence of Graphene. *Science* **2009**, *323*, 610−613.
(19) Sofo, J. O.; Chaudhari, A. S.; Barber, G. D. Graphane: A Two Dimensional Hydrocarbon. *Phys. Rev. B* **2007**, *75*, 153401.
(20) Guisinger, N. P.; Rutter, G. M.; Crain, J. N.; First, P. N.; Stroscio, J. A. Exposure of Epitaxial Grapheneon SiC(0001) to Atomic Hydrogen. *Nano Lett.* **2009**, *9*, 1462−1466.
(21) Sessi, P.; Guest, J. R.; Bode, M.; Guisinger, N. P. Patterning Graphene at the Nanometer Scale via Hydrogen Desorption. *Nano Lett.* **2009**, *9*, 4343−4347.
(22) Wojtaszek, M.; Tombros, N.; Caretta, A.; van Loosdrecht, P. H. M.; van Wees, B. J. A Road to Hydrogenating Graphene by a Reactive Ion Etching Plasma. *J. Appl. Phys.* **2011**, *110*, 063715.
(23) Luo, Z. Q.; Yu, T.; Kim, K. J.; Ni, Z. H.; You, Y. M.; Lim, S.; Shen, Z. X.; Wang, S. Z.; Lin, J. Y. Thickness-Dependent Reversible Hydrogenation of Graphene Layers. *ACS Nano* **2009**, *3*, 1781−1788.
(24) Xiang, H. J.; Kan, E. J.; Wei, S. H.; Gong, X. G.; Whangbo, M. H. Thermodynamically Stable Single-Side Hydrogenated Graphene. *Phys. Rev. B* **2010**, *82*, 165425.
(25) Cheng, S. H.; Zou, K.; Okino, F.; Gutierrez, H. R.; Gupta, A.; Shen, N.; Eklund, P. C.; Sofo, J. O.; Zhu, J. Reversible Fluorination of Graphene: Evidence of a Two-Dimensional Wide Bandgap Semiconductor. *Phys. Rev. B* **2010**, *81*, 205435.
(26) Zhou, J.; Liang, Q. F.; Dong, J. M. Enhanced Spin-Orbit Coupling in Hydrogenated and Fluorinated Graphene. *Carbon* **2010**, *48*, 1405−1409.
(27) Robinson, J. T.; Burgess, J. S.; Junkermeier, C. E.; Badescu, S. C.; Reinecke, T. L.; Perkins, F. K.; Zalalutdniov, M. K.; Baldwin, J. W.; Culbertson, J. C.; Sheehan, P. E.; Snow, E. S. Properties of Fluorinated Graphene Films. *Nano Lett.* **2010**, *10*, 3001−3005.
(28) Peelaers, H.; Hernandez-Nieves, A. D.; Leenaerts, O.; Partoens, B.; Peeters, F. M. Vibrational Properties of Graphene Fluoride and Graphane. *Appl. Phys. Lett.* **2011**, *98*, 051914.
(29) Ribas, M.; Singh, A.; Sorokin, P.; Yakobson, B. Patterning Nanorods and Quantum Dots on Fluorinated Graphene. *Nano Res.* **2011**, *4*, 143−152.
(30) Boukhvalov, D. W.; Katsnelson, M. I. Chemical Functionalization of Graphene. *J. Phys.: Condens. Matter* **2009**, *21*, 344205.
(31) Withers, F.; Dubois, M.; Savchenko, A. K. Electron Properties of Fluorinated Single-Layer Graphene Transistors. *Phys. Rev. B* **2010**, *82*, 073403.
(32) Bekyarova, E.; Itkis, M. E.; Ramesh, P.; Berger, C.; Sprinkle, M.; de Heer, W. A.; Haddon, R. C. Chemical Modification of Epitaxial Graphene: Spontaneous Grafting of Aryl Groups. *J. Am. Chem. Soc.* **2009**, *131*, 1336−1337.
(33) Kolb, H. C.; Finn, M. G.; Sharpless, K. B. Click Chemistry: Diverse Chemical Function from a Few Good Reactions. *Angew. Chem. Int. Ed.* **2001**, *40*, 2004−2021.
(34) Devadoss, A.; Chidsey, C. E. D. Azide-Modified Graphitic Surfaces for Covalent Attachment of Alkyne-Terminated Molecules by Click Chemistry. *J. Am. Chem. Soc.* **2007**, *129*, 5370−5371.
(35) Dreyer, D. R.; Park, S.; Bielaswki, C. W.; Ruoff, R. S. The Chemistry of Graphene Oxide. *Chem. Soc. Rev.* **2010**, *39*, 228−240.
(36) Kang, S. J.; Kocabas, C.; Ozel, T.; Shim, M.; Piparkar, N.; Alam, M. A.; Rotkins, S. V.; Rogers, J. A. High-Performance Electronics Using Dense, Perfectly Aligned Arrays of Single-Walled Carbon Nanotubes. *Nat. Nanotechnol.* **2007**, *2*, 230−236.
(37) Hassner, A.; Fowler, F. W. A General Synthesis of 2h-azirines from Olefins. Fused Azirines. *Tetrahedron Lett.* **1967**, *8*, 1545−1548.
(38) Clayden, J.; Greeves, N.; Warren, S. *Organic Chemistry*, 2nd ed.; Oxford University Press, Inc.: New York, 2012.
(39) Huisgen, R. 1,3 Dipolar Cycloaddition. *Proc. Chem. Soc.* **1961**, 357−361.
(40) Mondal, T.; Bhowmick, A. K.; Krishnamoorti, R. Chlorophenyl Pendant Decorated Graphene Sheet as a Potential Antimicrobial Agent: Synthesis and Characterization. *J. Mater. Chem.* **2012**, *22*, 22481−22487.
(41) Mondal, T.; Bhowmick, A. K. 2-Methyl Oxazoline-Grafted Carbon Nanofibers: Preparation, Characterization, and Their Role in Elastomeric Actuators. *J. Mater. Sci.* **2012**, *47*, 4178−4186.
(42) Clark, D. T.; Kilcast, D. Effect of Fluorine Substitution on the Molecular Core Binding Energies of Some Binuclear Aromatic Hydrocarbons. *J. Chem. Soc. B* **1971**, 2243−2247.
(43) Banwell, C.; McCash, E. *Fundamental of Molecular Spectroscopy*, 4th ed; Tata MacGraw Hill: New Delhi, 2004.
(44) Li, X.; Zhu, Y.; Cai, W.; Borysiak, M.; Han, B.; Chen, D.; Piner, R. D.; Colombo, L.; Ruoff, R. S. Transfer of Large-Area Graphene Films for High-Performance Transparent Conductive Electrodes. *Nano Lett.* **2009**, *9*, 4359−4563.
(45) Mondal, T.; Bhowmick, A. K.; Krishnamoorti, R. Synthesis and Characterization of Bi-Functionalized Graphene and Expanded Graphite using *n*-Butyl Lithium and Their Use for Efficient Water Soluble Dye Adsorption. *J. Mater. Chem. A* **2013**, *1*, 8144−8153.
(46) Mondal, T.; Bhowmick, A. K.; Krishnamoorti, R. Butyl lithium Assisted Direct Grafting of Polyoligomeric Silsesquioxane onto Graphene. *RSC Adv.* **2014**, *4*, 8649−8656.
(47) Balog, B.; Jorgensen, B.; Nilsson, L.; Andersen, M.; Rienks, E.; Bianchi, M.; Fanetti, M.; Lagsgaard, E.; Baraldi, A.; Lizzit, S.; Slijivancanin, Z.; Besenbachen, F.; Hammer, F.; Pedersen, T. G.; Hofmann, P.; Hornekar, L. Bandgap Opening in Graphene Induced by Patterned Hydrogen Adsorption. *Nat. Mater.* **2010**, *9*, 315−319.
(48) Shenoy, V. B.; Reddy, C. D.; Ramasubramaniam, A.; Zhang, Y. W. Edge-Stress-Induced Warping of Graphene Sheets and Nanoribbons. *Phys. Rev. Lett.* **2008**, *101*, 245501.
(49) Zhang, Y.; Brar, V. W.; Girit, C.; Zettl, A.; Cromie, M. F. Origin of Spatial Charge Inhomogeneity in Graphene. *Nat. Physics* **2009**, *5*, 722−726.
(50) Geringer, V.; Liebmann, M.; Echtermeyer, T.; Runte, S.; Schmidt, M.; Ruckamp, R.; Lemne, M. C.; Morgenstern, M. Intrinsic and extrinsic corrugation of monolayer graphene deposited on $SiO_2$. *Phys. Rev. Lett.* **2009**, *102*, 076102.
(51) Stokes, A. R.; Wilson, A. J. C. The Diffraction of X-rays by Distorted Crystal Aggregates. I. *Proc. Phys. Soc. London* **1944**, *56*, 174.
(52) Ryu, S.; Hau, M.; Maultzsch, J.; Heinz, T. F.; Kim, P.; Steigerwald, M. L.; Brush, L. E. Reversible Basal Plane Hydrogenation of Graphene. *Nano Lett.* **2008**, *8*, 4597−4602.
(53) Ferrari, A. C. Raman Spectroscopy of Graphene and Graphite: Disorder, Electron−Phonon Coupling, Doping, and Non-adiabatic Effects. *Solid State Commun.* **2007**, *143*, 47−57.

(54) Kawashima, Y.; Katagiri, G. Fundamentals, Overtones, and Combinations in the Raman Spectrum of Graphite. *Phys. Rev. B* **1995**, *52*, 10053−10059.
(55) Graf, D.; Molitor, F.; Ensslin, K.; Stampfer, C.; Jungen, A.; Hierold, C.; Wirtz, L. Spatially Resolved Raman Spectroscopy of Single and Few Layer Graphene. *Nano Lett.* **2007**, *7*, 238−242.
(56) Cançado, L. G.; Pimenta, M. A.; Neves, B. R. A.; Dantas, M. S. S.; Jorio, A. Influence of the Atomic Structure on the Raman Spectra of Graphite Edges. *Phys. Rev. Lett.* **2004**, *93*, 247401.
(57) Cheng, Y. C.; Huang, G. S.; Schwingenschlogl, U. Grüneisen Parameter of the G Mode of Strained Monolayer Graphene. *Phys. Rev. B* **2011**, *83*, 115449.
(58) Mohiuddin, T. M. G.; Lombardo, A.; Nair, R. R.; Bonetti, A.; Savini, G.; Jalil, R.; Bonini, N.; Basko, D. M.; Galiotis, C.; Marzar, N.; Novoselov, K. S.; Geim, A. K.; Ferrari, A. C. Uniaxial Strain in Graphene by Raman Spectroscopy: G Peak Splitting, Grüneisen Parameters, and Sample Orientation. *Phys. Rev. B* **2009**, *79*, 205433.
(59) Sakata, H.; Dresselhaus, G.; Dresselhaus, M. S.; Endo, M. Effect of Uniaxial Stress on the Raman. Spectra of Graphite Fibers. *J. Appl. Phys.* **1988**, *63*, 2769−2772.
(60) Bissett, M. A.; Tsuji, M.; Ago, H. Mechanical Strain of Chemically Functionalized Chemical Vapor Deposition Grown Graphene. *J. Phys. Chem. C* **2013**, *117*, 3152−3159.